



Australian Government
Bureau of Meteorology

The Centre for Australian Weather and Climate Research
A partnership between CSIRO and the Bureau of Meteorology



Convection and MJO Performance in UM7.1

Hongyan Zhu and Harry Hendon

CAWCR Technical Report No. 022

April 2010



www.cawcr.gov.au



Convection and MJO Performance in UM7.1

Hongyan Zhu ¹ and Harry Hendon ¹

¹*Centre for Australian Weather and Climate Research*

CAWCR Technical Report No. 022

April 2010

ISSN: 1836-019X

National Library of Australia Cataloguing-in-Publication entry

Title: Convection and MJO Performance in UM7.1 [electronic resource] / Hongyan Zhu and Harry Hendon.

ISBN: 978-1-921605-70-3 (PDF)

Series: CAWCR technical report; 22.

Notes: Bibliography.

Subjects: Australia—Convection (Meteorology)--Mathematical models.

Other Authors/Contributors: Hendon, Harry

Enquiries should be addressed to:
Dr. Hongyan zhu
Centre for Australian Weather and Climate Research:
A partnership between the Bureau of Meteorology and CSIRO
GPO Box 1289 Melbourne
Victoria 3001, Australia

H.Zhu@bom.gov.au

Copyright and Disclaimer

© 2010 CSIRO and the Bureau of Meteorology. To the extent permitted by law, all rights are reserved and no part of this publication covered by copyright may be reproduced or copied in any form or by any means except with the written permission of CSIRO and the Bureau of Meteorology.

CSIRO and the Bureau of Meteorology advise that the information contained in this publication comprises general statements based on scientific research. The reader is advised and needs to be aware that such information may be incomplete or unable to be used in any specific situation. No reliance or actions must therefore be made on that information without seeking prior expert professional, scientific and technical advice. To the extent permitted by law, CSIRO and the Bureau of Meteorology (including each of its employees and consultants) excludes all liability to any person for any consequences, including but not limited to all losses, damages, costs, expenses and any other compensation, arising directly or indirectly from using this publication (in part or in whole) and any information or material contained in it.

Contents

Abstract.....	1
1. Introduction.....	3
2. Evaluation of MJO in UM.....	4
3. Convection behaviour in UM.....	8
3.1 Relationship between saturation fraction and precipitation.....	8
3.2 Thermal dynamic feature related to the intensive precipitation.....	9
3.2.1 Moisture anomaly.....	9
3.2.2 Temperature anomaly.....	10
3.2.3 Zonal wind anomaly.....	11
3.2.4 Latent heat flux.....	13
4. Conclusion and future work.....	13
References.....	14

List of Figures

Fig. 1	For observation. Space–time spectral density (contours) and signal strength (shading) of symmetric precipitation (a) and U850 (b) (2.5°–10° latitude). Contour interval in (a) is 2.5×10^{-4} fractional power per unit frequency per unit wavenumber (first three thin contours at 0.3125×10^{-4} , 0.625×10^{-4} , and 1.25×10^{-4}) and in (b) contour interval is 2×10^{-3} with first three thin contours at 1×10^{-3} , 0.5×10^{-3} , and 0.25×10^{-3} . Signal strength shading level is 0.1 with first level at 0.2, which is deemed significant at the 99% level. Dispersion curves are shown for Kelvin waves with equivalent depths of 10, 40, and 200 m; equatorial Rossby waves with equivalent depths of 20 and 40 m and external Rossby–Haurwitz waves for equivalent depth of 10 km; and meridional mode $n = 1$ and $n = 3$	4
Fig. 2	As in Fig. 1, but for UM7.1 (a,b) and SP-CAM (c,d)	5
Fig. 3	Averaged precipitation variance for (a) observation, (b) UM7.1 and (c) SP-CAM. ...	6
Fig. 4	Averaged 30-90 days filtered precipitation variance for (a) observation (b) um7.1 and (c) SP-CAM	7
Fig. 5	(a) Mean daily precipitation composited into 5 % bins of saturation fraction for observation, UM7.1 and SP-CAM. (b) Ratio of number of data points in each bin to the total number of data points.....	8
Fig. 6	Daily mean moisture anomaly composited by the occurrence of daily mean precipitation rate anomaly greater than 9.6 mm / day for (a) OBS; (b) UM7.1; and (c) SP-CAM.	10
Fig. 7	Daily mean temperature anomaly composited by the occurrence of daily mean precipitation rate anomaly greater than 9.6 mm / day for (a) OBS; (b) Hadgem3; and (c) SP-CAM.	11
Fig. 8	Daily mean zonal wind anomaly composited by the occurrence of daily mean precipitation rate anomaly greater than 9.6 mm / day for (a) OBS; (b) UM7.1; and (c) SP-CAM.	12
Fig. 9	Daily latent heat flux anomaly composited by the occurrence of daily mean precipitation rate anomaly greater than 9.6 mm / day for (a) OBS; (b) Hadgem3; and (c) SP-CAM.	13

ABSTRACT

Variability associated with the Madden-Julian Oscillation (MJO) in the latest version of the UK Met Office Unified model (UM7.1) is evaluated by comparing to observations and a cloud-resolved model, in which a 2-dimension cloud resolving model replacing the convective parameterization scheme. To better understand the cause of the poor simulation of the MJO in UM, diagnosing the behaviour of convection on the model grid scale is carried out in this paper.

This work shows that in the UM the following features of convection associated with the MJO are not well represented:

- 1) There is still convection occurring in the relatively dry environment, and also the precipitation stops growing after reaching 85% of the saturation fraction value.
- 2) The model fails to produce the pre-moistening by shallow convection before intensive rainfall events and rapid drying after the intensive rainfall event by the meso-scale downdrafts.
- 3) There is lack of baroclinic nature of zonal wind associated with the deep convection, which could be due to the parameterised momentum transfer in the model.
- 4) The latent heat flux anomaly associated with intense rainfall events is only about half value of those from observation and cloud resolved model.

1. INTRODUCTION

Realistic simulation of the MJO using global climate models continues to be a challenge (e.g. Kim et al. 2009). Several studies have highlighted the great sensitivity of the simulation of the MJO to the details of convection parameterizations, thus suggesting that deficiencies in the representation of tropical convection may be the primary contributor to the poor simulations. However, these studies have provided conflicting results as to where the problem may be. For example, Slingo et al. (1996) suggested that convection schemes closed on buoyancy tended to simulate stronger MJO variability, whereas Lin et al. (2006) suggested that models with moisture convergence closure simulated better MJO variability. Other studies have indicated that a successful simulation of the MJO depends on the specific details of the representation of the complex interactions of convection with other physical processes in the model. For instance, some studies have suggested that an improved MJO simulation results from convective parameterizations that employ inhibition mechanism (Tokioka et al. 1988; Wang and Schlesinger 1999; Lee et al. 2001; Maloney and Hartmann 2001; Maloney 2002; Lee et al. 2003; Zhang and Mu 2005; Lin et al. 2008), while others have pointed to an improved representation of downdrafts and rain re-evaporation (Maloney and Hartmann 2001).

These wide ranging and sometimes conflicting results make it difficult to identify why one scheme works and another does not. In order to expedite the improvement of the model simulations of the MJO, some basic diagnostics of the simulated convection are required that are aimed at revealing the model's ability to simulate the key crucial processes that are fundamental to the MJO. Zhu et al. (2009) have proposed some simple diagnostics aimed to do just that. They studied the simulation of the MJO using the same GCM (NCAR Community Model, CAM model), but with two very different treatments of convection. The MJO was essentially absent from the simulation that used the Zhang and McFarland (1995) mass flux convection scheme (we refer to this simulation as CAM), while a strong MJO-like phenomena was simulated in the other model that treated the parameterization of convective processes with the super-parameterized 2D cloud resolving model (SP-CAM; Grabowski 2001; Khairoutdinov and Randall 2001; Khairoutdinov et al. 2005). Analysis of the differences in behaviour of convection on the model grid-scale in the two simulations indicated that an improved simulation of the MJO might depend on the simulated convection exhibiting certain observed characteristics, including:

- 1) precipitation should be an exponentially increasing function of the column saturation fraction;
- 2) heavy precipitation should be associated with a stratiform diabatic heating profile;
- 3) there should be a positive co-variance of precipitation with surface latent heat flux.

A natural extension of Zhu et al. (2009), who examined MJO/convection behaviour in a single model but with two vastly different treatments of convective processes, is to apply the techniques to a wider range of models. In the present work, we apply the diagnostic methods from Zhu et al. to the climate model simulation from UM 7.1 (the latest version Unified Model developed at UK Met Office), with an aim to evaluate and ultimately improve the representation of convective processes that are required for a faithful simulation of the MJO.

In the present study, the model results are compared to observations and also to the results from SP-CAM. The observation data sets for verification in this paper include the Global Precipitation Climatology Project (GPCP) daily precipitation analysis with 1 degree resolution (Adler et al. 2003), daily mean latent heat flux from the Woods Hole Oceanographic Institution (WHOI) Objectively Analyzed air-sea Fluxes Project (OAFlux; Yu et al. 2008), also with 1 degree resolution, and the European Centre for Medium Range Weather Forecasts 40-year re-analysis (ERA40) of daily mean winds, temperature and moisture fields with 2.5 degree resolution (Uppala et al. 2005). We use daily data covering the period from July 1998 to June 2002 (the period of available SP-CAM simulations).

2. EVALUATION OF MJO IN UM

The simulation of the MJO is first assessed by examination of the space-time spectral density and signal strength of equatorially symmetric precipitation and U850 (symmetric latitudes 2.5–10 degree) following Hendon and Wheeler (2008). The observed spectra of rainfall (Fig. 1a) and U850 (Fig. 1b) exhibit pronounced peaks at eastward wavenumbers 1–3 (rainfall) and wavenumber 1 (U850) for periods centered on about 50 d. This spectral peak is regarded to be associated with the MJO (Salby and Hendon 1994) and it is seen to be well removed and distinct from the spectral peaks associated with higher frequency Kelvin waves (eastward wavenumbers 1–10 with periods less than ~15 days; e.g., Wheeler and Kiladis 1999). A similar analysis of UM7.1 (Fig. 2a,b) reveals an absence of a strong spectral peak with significant “signal strength” associated with the MJO. A realistic spectrum of higher frequency Kelvin waves is simulated, but at the lower eastward frequencies associated with the MJO, the spectrum from UM7.1 appears mostly red, with no strong evidence of an intraseasonal spectral peak especially in rainfall. For comparison, we show the spectra from SP-CAM (Fig. 2c,d), which exhibits a pronounced spectral peak associated with the MJO in both rainfall and U850 but a weaker spectrum of higher frequency Kelvin waves.

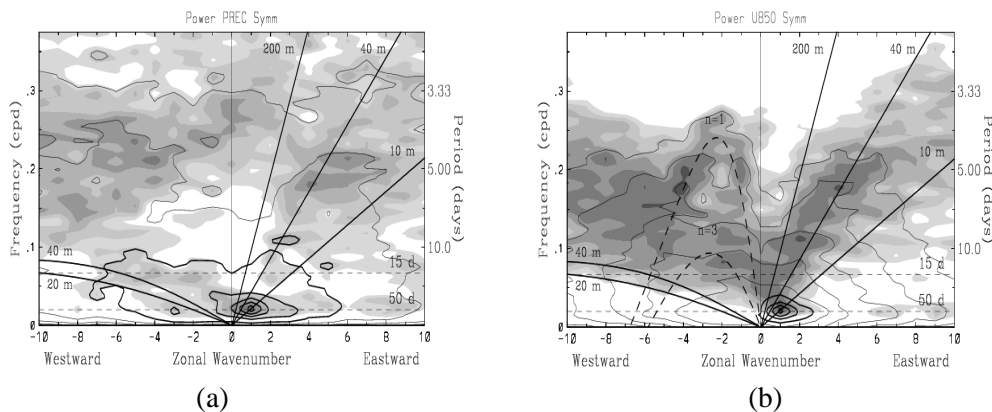


Fig. 1 For observation. Space–time spectral density (contours) and signal strength (shading) of symmetric precipitation (a) and U850 (b) (2.5°–10° latitude). Contour interval in (a) is 2.5×10^{-4} fractional power per unit frequency per unit wavenumber (first three thin contours at 0.3125×10^{-4} , 0.625×10^{-4} , and 1.25×10^{-4}) and in (b) contour interval is 2×10^{-3} with first three thin contours at 1×10^{-3} , 0.5×10^{-3} , and 0.25×10^{-3} . Signal strength shading level is 0.1 with first level at 0.2, which is deemed significant at the 99% level. Dispersion curves are shown for Kelvin waves with equivalent depths of 10, 40, and 200 m; equatorial

Rossby waves with equivalent depths of 20 and 40 m and external Rossby–Haurwitz waves for equivalent depth of 10 km; and meridional mode $n = 1$ and $n = 3$.

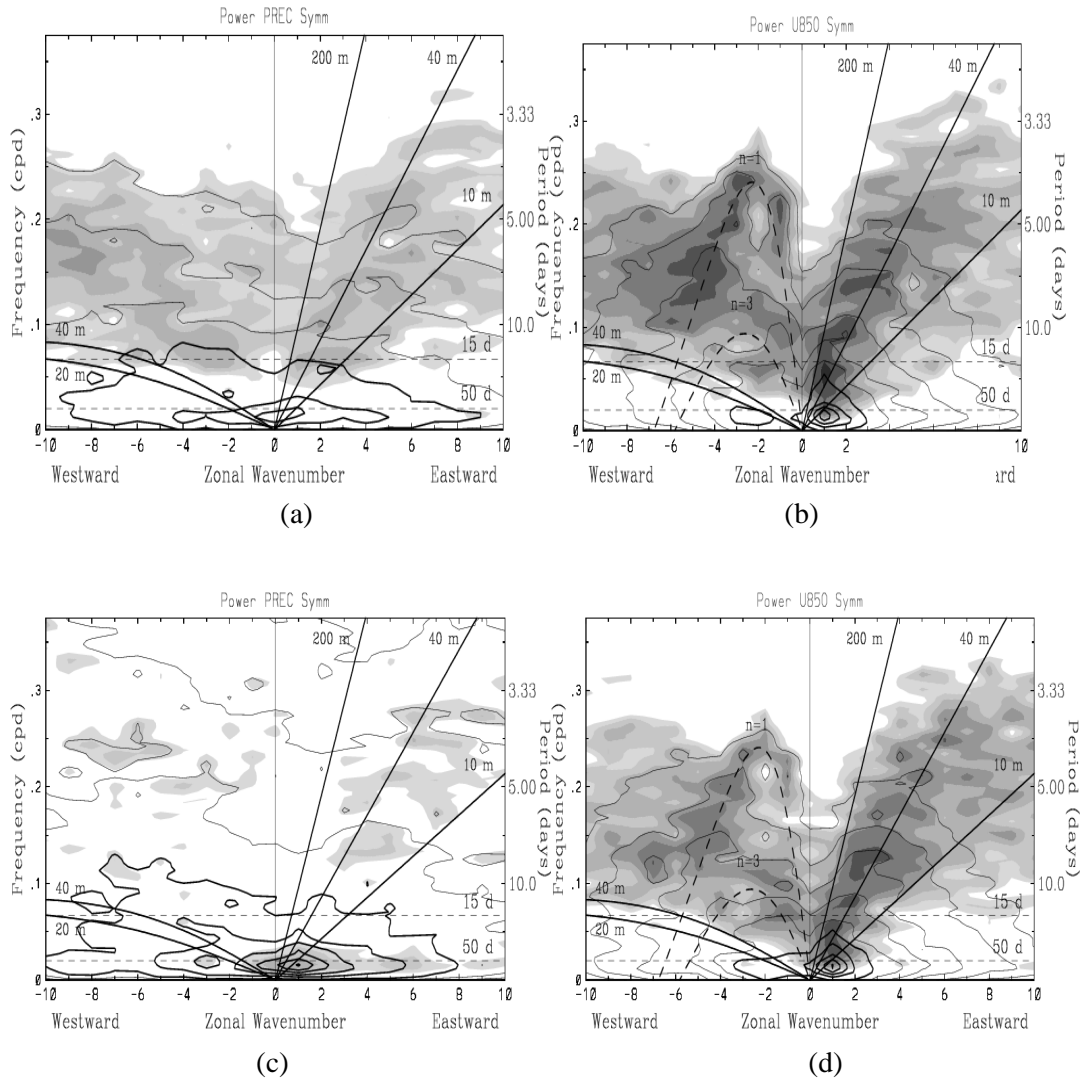
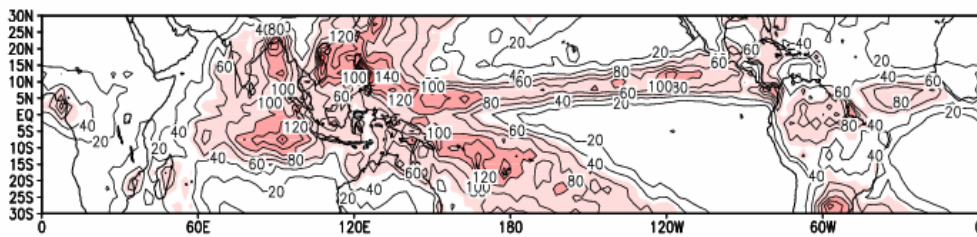
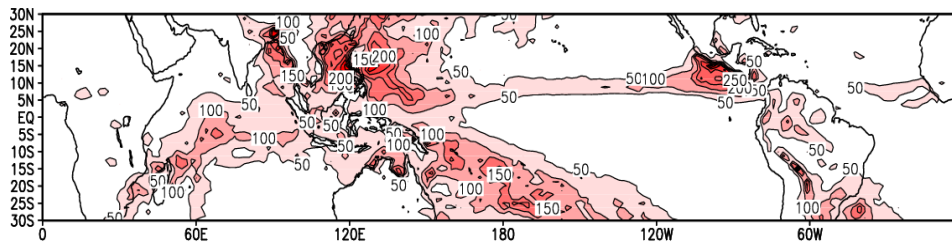
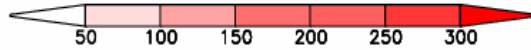


Fig. 2 As in Fig. 1, but for UM7.1 (a,b) and SP-CAM (c,d) .

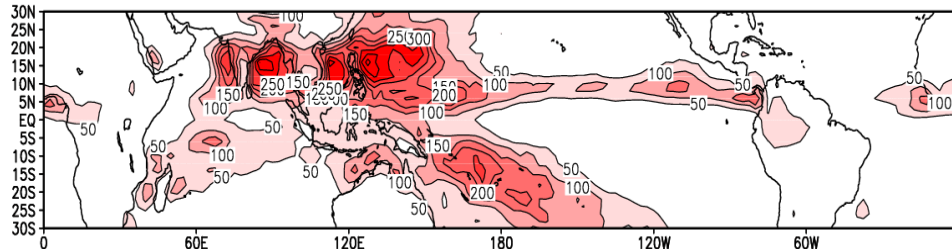
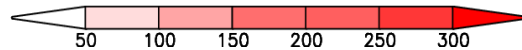
Further investigation of the spatial distribution of rainfall variance (Fig. 3) reveals some additional deficiencies that may contribute to the lack of a MJO in the UM7.1 simulation: rainfall variance in UM7.1 is about 30 degree west comparing to the observation in the tropical Indian Ocean, which is thought to be the incipient region for the MJO. From observations, we see that the local maximum of rainfall variance in the Indian Ocean is of a similar magnitude to the local maximum in the western Pacific, although the maximum in the west Pacific occurs in the north and south convergence zones (which UM7.1 captures), where as there is a single near-equatorial maximum in the Indian Ocean at about 95 E. In SP-CAM and UM7.1, the location of variance in the Indian Ocean is located further to the west comparing to the observation, at about 65E, and we see that rainfall variance is spuriously large to the north of the equator in SP-CAM.



(a)



(b)



(c)

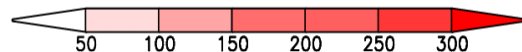
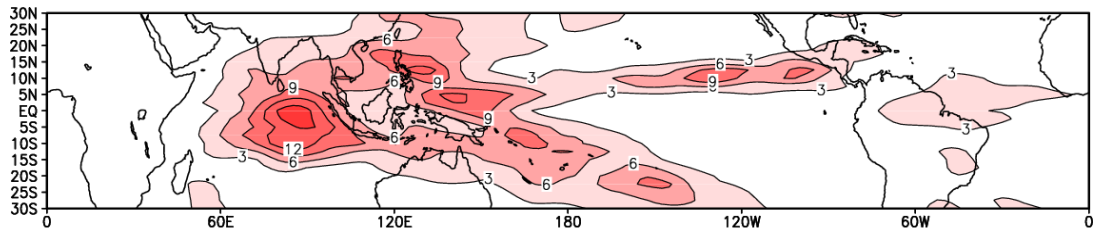
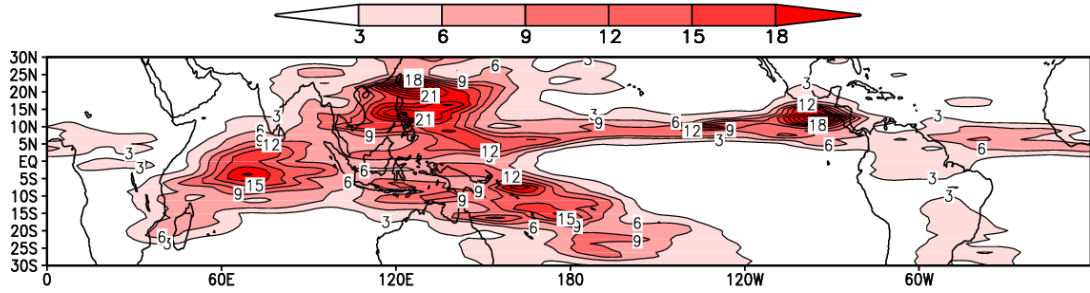


Fig. 3 Averaged precipitation variance for (a) observation, (b) UM7.1 and (c) SP-CAM.

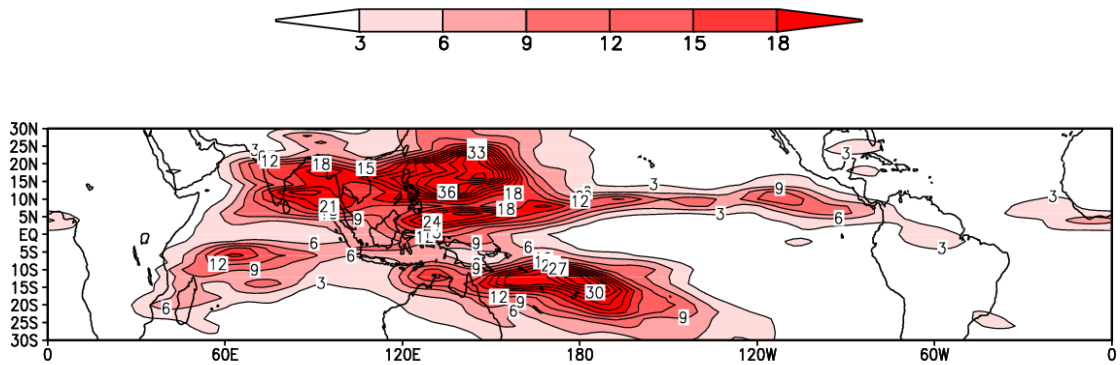
A further decomposition of the rainfall variance to MJO frequencies (Fig. 4) emphasizes the location of MJO signal in the Indian Ocean is further west and south comparing to the position of variance from observation in both of UM7.1 and SP-CAM, and in the Western Pacific there is spuriously strong off-equatorial variability in SP-CAM. We now attempt to better understand the cause of the poor simulation of the MJO in UM7.1 by diagnosing the behaviour of convection on the model grid scale as in Zhu et al. (2009).



(a)



(b)



(c)

Fig. 4 Averaged 30-90 days filtered precipitation variance for (a) observation (b) um7.1 and (c) SP-CAM

3. CONVECTION BEHAVIOUR IN UM

3.1 Relationship between saturation fraction and precipitation

Bretherton et. al (2004), using satellite-observed rainfall and humidity, showed an quasi-exponential relationship between daily variations of precipitation and saturation fraction, which is the ratio of the column integrated mixing ratio to the column integrated saturated mixing ratio. The rainfall rate at a grid point (typically $\sim 200\text{km} \times 200\text{km}$) is a strong increasing function of column saturation fraction. We reproduce the results of Bretherton et al (2004) using daily GPCP rainfall and ERA-40 humidity and temperatures for ocean grid points in the region 60°E - 180°E and 20°S - 20°N (Fig. 5). Nonzero precipitation occurs after about 0.5 saturation fraction, followed by a quasi-exponential increase up to 95% saturation. In SP-CAM, the rapid increase of precipitation starts at a greater saturation fraction compared to observation (0.7 compared to 0.6) then the precipitation rate increases at a much higher rate. The behaviour of rainfall with saturation fraction in UM7.1 is similar to SP-CAM, but the increase begins at a more realistic 0.6 saturation fraction. And, rainfall in UM7.1 appears to tail off for saturation fractions above 0.85.

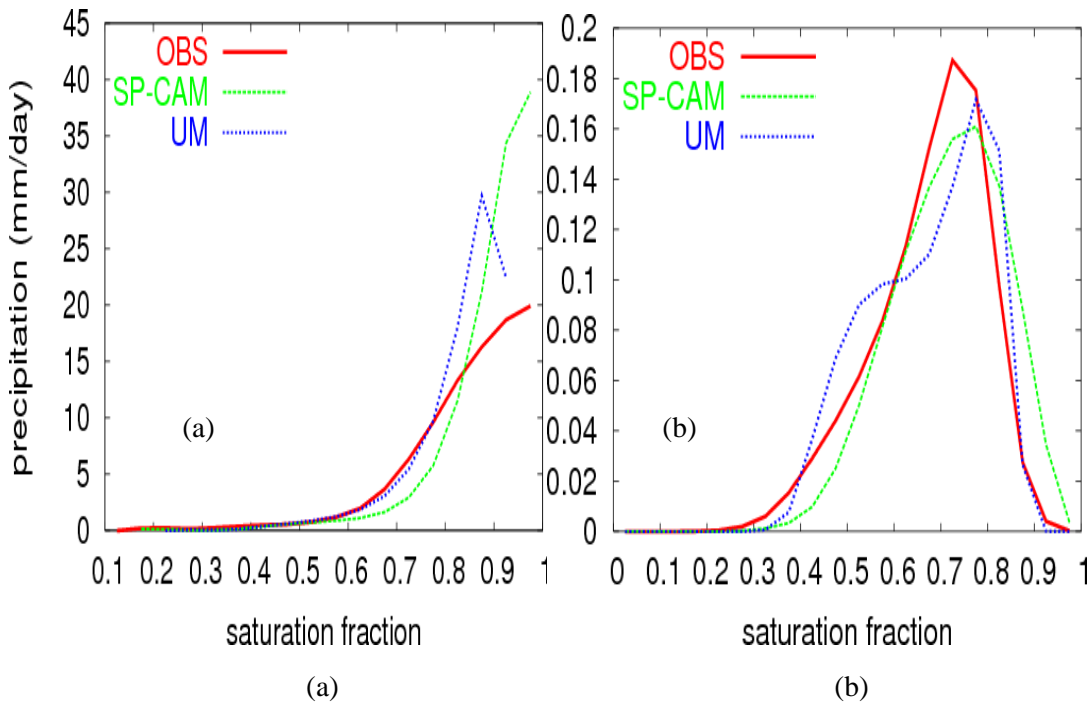


Fig. 5 (a) Mean daily precipitation composited into 5 % bins versus saturation fraction for observation, UM7.1 and SP-CAM. (b) Ratio of number of data points in each bin to the total number of data points.

We also calculate the numbers of occurrences of precipitation in each bin of saturation fraction (Fig. 5b). For observations, the mode occurs at 0.7 saturation fraction, followed by the rapid decrease towards the higher values of saturation fraction. In SP-CAM, the distribution is quite close to the observation; except that there are more cases for saturation fraction bigger than

0.80. The UM7.1 simulation exhibits two peaks, one near 0.45 and one near 0.8, indicating a tendency in UM7.1 to develop convection at too many grid points with moderate saturation.

3.2 Thermal dynamic feature related to the intensive precipitation

Zhu et al. (2009) have stated that the structure of anomalies of moisture and temperature associated with the MJO can be inferred from the daily behaviour based on the unfiltered analysis. They concluded that the convection features associated with MJO filtered precipitation is consistent with those associated with 5th rainfall quintile. Therefore in this part, we only study the convection behaviour in UM related with the intensive rainfall events to try to understand the different relationship between precipitation and grid column relative humidity in Fig. 5.

3.2.1 Moisture anomaly

To isolate intense precipitation events, we calculate the precipitation anomaly by removing the annual mean and seasonal cycle. An intense rainfall event is defined when the precipitation anomaly is bigger than one standard deviation of observed value, which is about 9.65 mm/d. In Fig. 6, we composite moisture anomaly relative to the intensive precipitation events.

Observation shows that starting at -12 day, there is a gradual moistening with depth before the maximum precipitation anomaly, indicating shallow convection pre-moistening the grid column and providing a favourable condition for the later deep convection development. The moisture anomaly has a maximum value at day 0 at the middle troposphere. The drying starts at day 5 in the boundary layer, extending upwards to the lower troposphere at day 10. Similar to the observed MJO behaviour (Benedict and Randall, 2007), the moisture recharge time is longer than the moisture dis-charge time in the lower troposphere due to the meso-scale downdraft which dries the lower troposphere quickly after the intense precipitation peak.

In UM7.1, there is no obvious moistening tendency of shallow convection before deep convection. The deep convection moistening starts at around -7 day relative to rainfall anomaly maximum, and the amplitude increases with increasing precipitation, reaching the maximum at day 0 at the height of 700hPa. The moisture anomaly distribution is rather symmetric relative to day 0. The moisture dis-charge time is slightly longer than the moisture re-charge time, especially in the boundary layer.

For the SP-CAM, the moistening of troposphere occurring between -17 day to +20 day, much longer comparing to observation and UM7.1. There is no obvious pre-moistening of shallow convection too, and the pattern of moistening has an onion shape starting at the middle troposphere. As discussed in paper (Zhu et. al. 2009), for SP-CAM, 4km resolution might not be able to resolve shallow convection sufficiently well to produce an earlier moistening of the lower troposphere as the observed before the maximum precipitation occurring. This also indicates that in SP-CAM pre-moistening of shallow convection may not be a critical factor for the strong MJO.

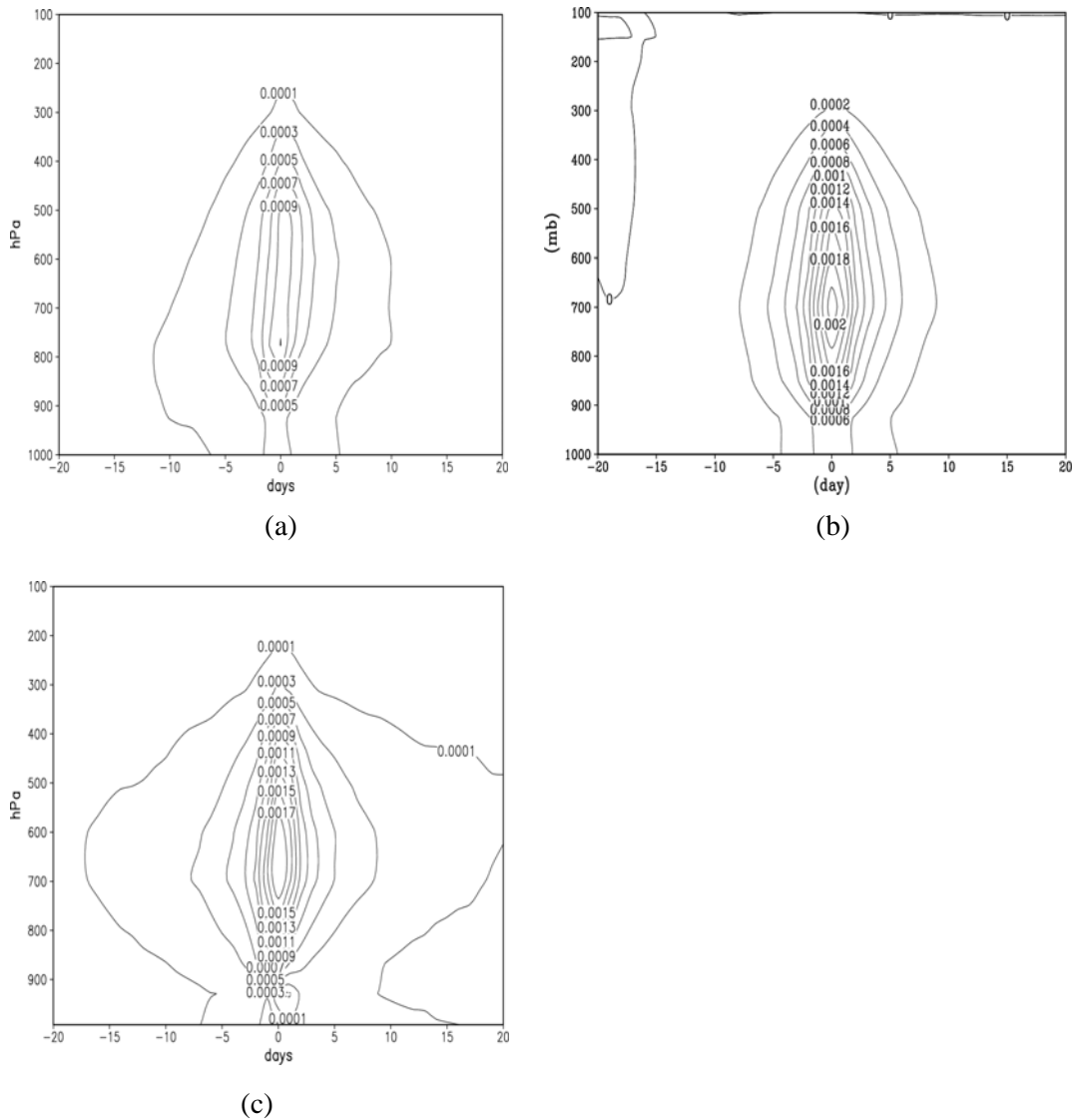


Fig. 6 Daily mean moisture anomaly composited by the occurrence of daily mean precipitation rate anomaly greater than 9.6 mm / day for (a) OBS; (b) UM7.1; and (c) SP-CAM.

3.2.2 Temperature anomaly

Similar to Fig. 6, Fig. 7 shows that lag relationship of the temperature anomaly relative to the intense rainfall events. For the temperature field, in observation, there is positive anomaly at the upper troposphere and negative anomaly in the lower troposphere and near the surface. This top heavy temperature profile is consistent with the stratiform precipitation heating profile, indicating there is stratiform precipitation within the deep convective regime. The cooling anomaly in the lower layer and warming anomaly in the upper layer indicates that the atmosphere is stable to convection at the time of the precipitation maximum.

Both UM 7.1 and SP-CAM is able to reproduce the observed temperature profile, but in SP-CAM the cooling tendency in the boundary layer is much stronger probably due to the too active downdraft evaporation cooling.

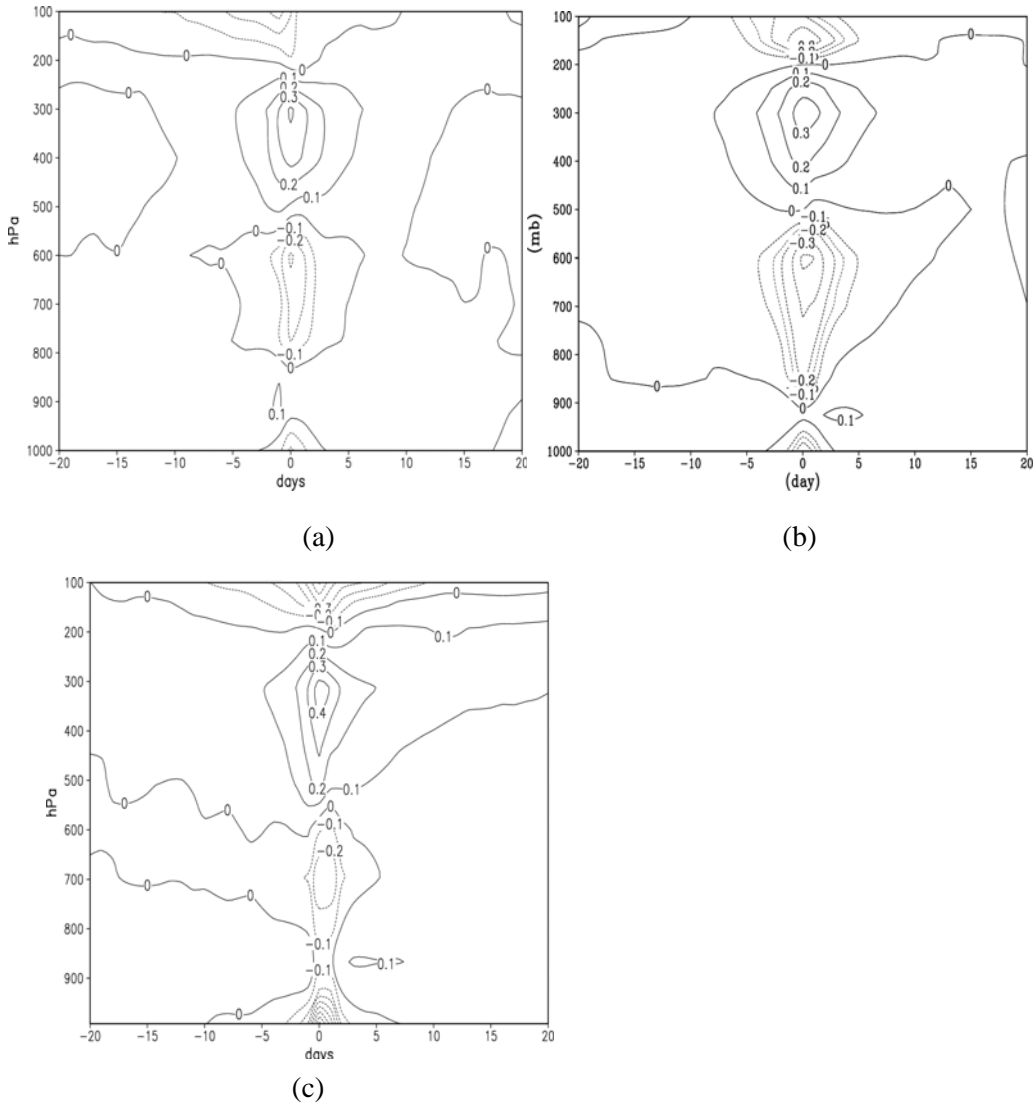


Fig. 7 Daily mean temperature anomaly composited by the occurrence of daily mean precipitation rate anomaly greater than 9.6 mm / day for (a) OBS; (b) Hadgem3; and (c) SP-CAM.

3.2.3. Zonal wind anomaly

To understand the zonal wind structure associate with convection, in Fig 8, we composite the wind anomaly for the rainfall events when the precipitation anomaly greater than 9.65 mm/d.

Observation of zonal wind anomaly relative to strong precipitation anomaly shows that there is a baroclinic wind structure associated with deep convection heating source, with east wind transition to west wind near the surface between -5 day and 0 day.

The zonal wind in UM7.1 is able to capture the east and west wind transition, but has a more barotropic structure comparing to observation. Including momentum transport in UM could be a reason for the more barotropic nature of the zonal wind in UM simulation. Another difference from the observation is that weak westerly wind anomaly is only confined in the boundary layer after day 10 in UM simulation.

SP-CAM reproduces the baroclinic wind feature and east and west transition near the surface reasonably well, except that the maximum west wind occurs rather earlier, shortly after the rainfall maximum above the boundary layer.

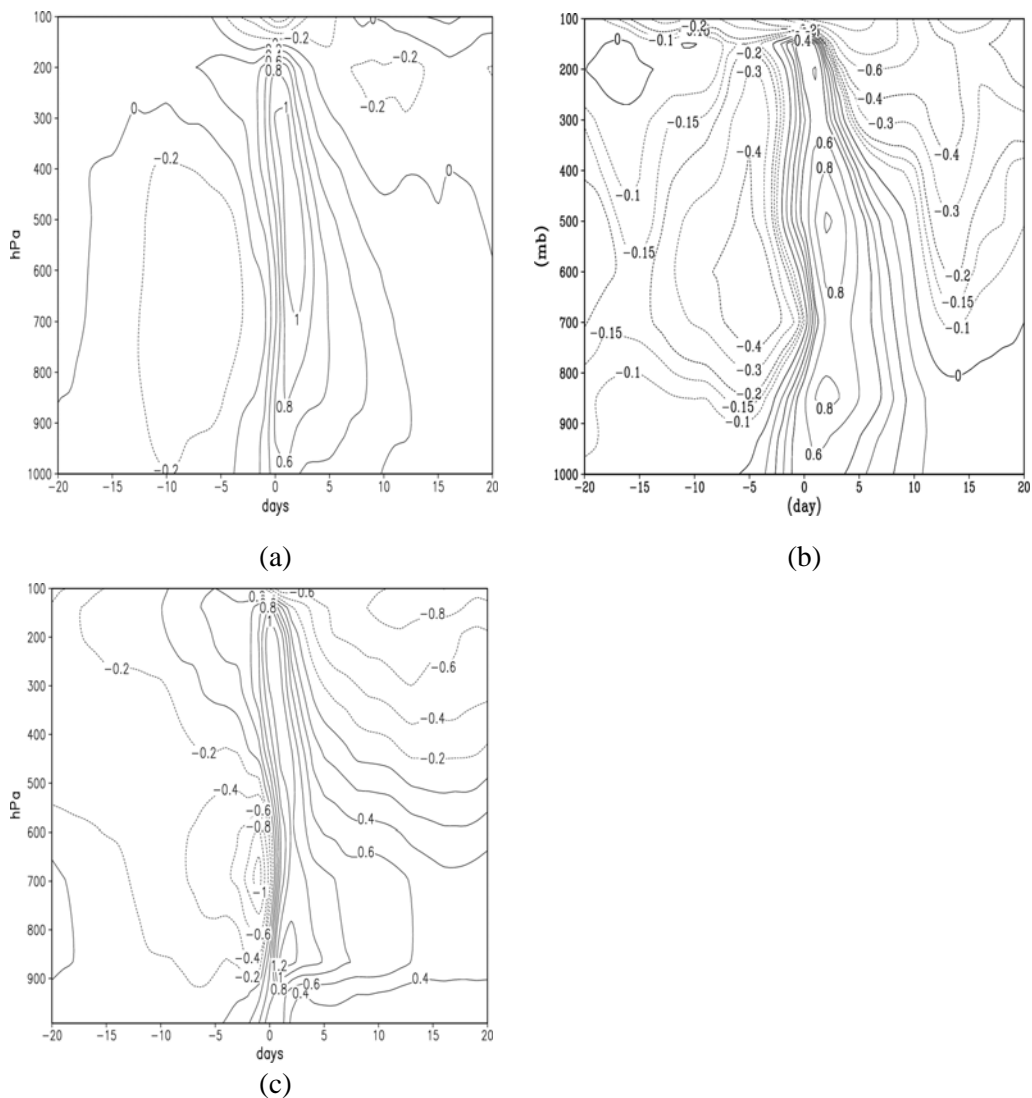


Fig. 8 Daily mean zonal wind anomaly composited by the occurrence of daily mean precipitation rate anomaly greater than 9.6 mm / day for (a) OBS; (b) UM7.1; and (c) SP-CAM.

3.2.4. Latent heat flux

Latent heat flux is the mechanism which generates and maintains the instability for the tropical convection; therefore we are also interested to compare latent heat flux changes during the strong rainfall events.

For observation (Fig. 9), latent heat flux started to increase at about -7 day and peaks at the same time when the precipitation anomaly reaches the maximum. In UM7.1, latent heat flux is positively correlated with rainfall anomaly, and peaks simultaneously with precipitation as the observation except that the maximum amplitude is smaller, about half value of the observation. In SP-CAM, the latent heat flux anomaly lags about one day relative to the rainfall maximum, reflecting the fact that the rainfall variation is dominated by the over strong MJO events in this model.

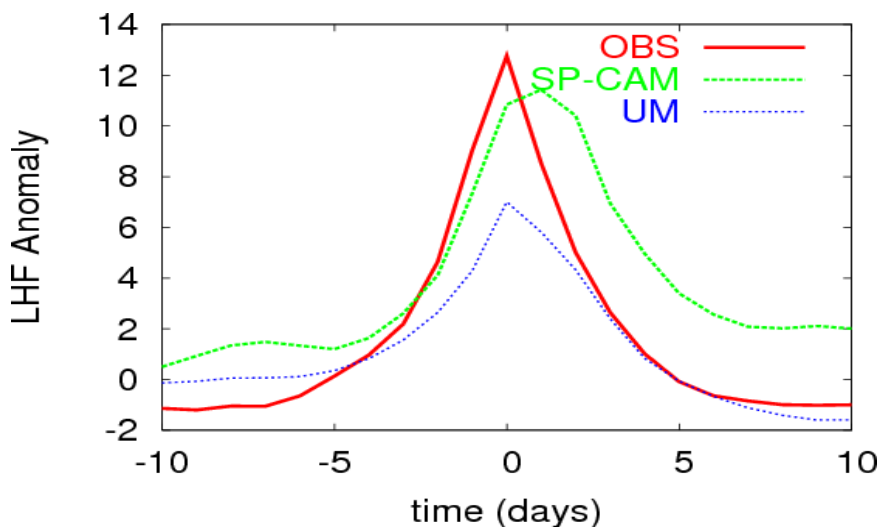


Fig. 9 Daily latent heat flux anomaly composited by the occurrence of daily mean precipitation rate anomaly greater than 9.6 mm / day for (a) OBS; (b) Hadgem3; and (c) SP-CAM.

4. CONCLUSION AND FUTURE WORK

MJO simulation and associated convection features in UM7.1 are compared with observation and SP-CAM.

The power spectrum analysis reveals an absence of a spectral peak associated with the MJO in UM7.1. A realistic spectrum of higher frequency Kelvin waves is simulated, but there is no evidence of an intraseasonal spectral peak in either rainfall or U850. In UM7.1 rainfall variance in the tropical Indian Ocean is about 30 degree west relative to the location where the centre of rainfall variance is in the observation, at about 95E, which is thought to be the incipient region for the MJO.

To better understand the cause of the poor simulation of the MJO in UM7.1, we diagnose the behaviour of convection on the model grid scale as in Zhu et al. (2009).

UM7.1 is able to reproduce a positive/negative temperature anomaly couplet during heavy rainfall possibly indicative of the presence of a stratiform diabatic heating profile.

We also show that in UM7.1 following features of convection are not well represented in the model.

- 1) There is still convection occurring in the relatively dry environment, and also the precipitation stops growing after reaching 85% of the saturation fraction value;
- 2) The model fails to produce the pre-moistening by shallow convection before intensive rainfall events and rapid drying after the intensive rainfall event by the meso-scale downdrafts;
- 3) There is lack of baroclinic nature of zonal wind associated with the deep convection, which could be due to the parameterised momentum transfer in the model;
- 4) The latent heat flux anomaly associated with maximum precipitation anomaly is only about half value of those observed and in SP-CAM.

Based on the above finding, our future work will carry on sensitivity studies to investigate which aspects of convection feature are associated with the weak MJO simulation in UM7.1 and make modifications accordingly to improve MJO in the model simulation. For example, to suppress the convection events in the relatively dry environment, we could restrict the triggering of convection to higher saturation fraction value; to have a gradual moisture recharge associated with strong precipitation and rapid moisture discharge afterwards, there is a need to increase the pre-moistening effect of shallow convection and post-drying effects of downdraft; to reduce the barotropic feature of zonal wind structure associated with deep convection, we could reduce the momentum transport effect in the convection scheme for deep convection. We also need to understand causes for the weak latent heat flux during the intense rainfall events in UM7.1.

REFERENCES

- Adler, R.F., Huffman, G.J., Chang, A., Ferraro, R., Xie, P., Janowiak, J., Rudolf, B., Schneider, U., Curtis, S., Bolvin, D., Gruber, A., Susskind, J. and Arkin, P. 2003: The Version 2 Global Precipitation Climatology Project (GPCP) Monthly Precipitation Analysis (1979-Present). *J. Hydrometeorol.*, **4**, 1147-1167.
- Benedict, J. and Randall, D. 2007: Observed characteristics of the MJO relative to maximum rainfall. *J. Atmos. Sci.*, **64**, 2332-2354.
- Bretherton, C., Peters, M. E. and Back, L. 2004: Relationships between water vapor path and precipitation over the tropical oceans. *J. Climate*, **17**, 517-1528.
- Grabowski, W. W. 2001: Coupling cloud processes with the large-scale dynamics using the Cloud-Resolving Convection Parameterization (CRCP). *J. Atmos. Sci.*, **58**, 978-997.

- Hendon, H. H., and Wheeler, M. C. 2008: Some space-time spectral analyses of tropical convection and planetary-scale waves, *Journal of the Atmospheric Sciences*, **65**, 2936-2948.
- Khairoutdinov, M. and Randall, D. 2001: A cloud resolving model as a cloud parameterization in the NCAR Community Climate System Model: Preliminary results. *Geophys. Res. Lett.* **28**, 3617-3620.
- Khairoutdinov, M., Randall, D. and Demott, C. 2005: Simulations of the Atmospheric general circulation using a cloud-resolving model as a superparameterization of physical processes. *J. Atmos. Sci.* **62**, 2136-2154.
- Kim, D. and co-authors, 2009: Application of MJO simulation diagnostics climate models. *J. Climate*, (accepted).
- Lee, M. I., Kang, I. S., Kim, J. K. and Mapes, B. E. 2001: Influence of cloud-radiation interaction on simulating tropical intraseasonal oscillation with an atmospheric general circulation model, *J. Geoph. Res. - Atmos.*, *106*(D13), 14219-14233.
- Lee, M. I., Kang, I. S. and Mapes, B. E. 2003: Impacts of cumulus convection parameterization on aqua-planet AGCM Simulations of tropical intraseasonal variability, *Journal of the Meteorological Society of Japan*, *81*(5), 963-992.
- Lin, H., Brunet, G. and Derome, J. 2008: Forecast skill of the Madden–Julian oscillation in two Canadian atmospheric models. *Mon. Wea. Rev.*, **136**, 4130–4149.
- Lin, Jia-lin, and Coauthors, 2006: Tropical intraseasonal variability in 14 IPCC AR4 climate models. Part I: convective signals. *J. Climate*, **19**, 2665-2690.
- Maloney, E. and Hartmann, D. 2001: The sensitivity of intraseasonal variability in NCAR CCM3 to changes in convective parameterization. *J. Climate*, **14**, 2015-2034.
- Maloney, E. D. 2002: An intraseasonal oscillation composite life cycle in the NCAR CCM3.6 with modified convection, *J. Clim.*, **15**(9), 964-982.
- Raymond, D. J., 1995: Regulation of moist convection over the West Pacific warm pool. *J. Atmos. Sci.*, **52**, 3945-3959.
- Raymond, D. J and Fuchs, Z. 2009: Moisture modes and the Madden-Julian oscillation. *J. Climate*, (in press).
- Salby, M.L. and Hendon, H.H. 1994: Intraseasonal behaviour of winds, temperature and convection in the tropics. *J. Atmos. Sci.*, **51**, 2207-2224.
- Slingo, J. M., and Coauthors, 1996: Intraseasonal oscillations in 15 atmospheric general circulation models: Results from an AMIP diagnostic subproject. *Climate Dyn.*, **12**, 325-357.

- Tokioka, T., Yamasaki, K., Kitoh, A. and Ose, T. 1988: The equatorial 30-60 day oscillation and the Arakawa-Schubert penetrative cumulus parameterization. *J. Meteor. Soc. Japan*, **66**, 883-901.
- Wang, W. and Schlesinger, M. E. 1999: The dependence on convective parameterization of the tropical intraseasonal oscillation simulated by the UIUC 11-layer atmospheric GCM. *J. Climate*, **12**, 1423-1457.
- Yu, L., Jin, X. and Weller, R. A. 2008: Multidecade Global Flux Datasets from the Objectively Analyzed Air-sea Fluxes (OAFlux) Project: Latent and sensible heat fluxes, ocean evaporation, and related surface meteorological variables. *Woods Hole Oceanographic Institution, OAFlux Project Technical Report. OA-2008-01*, 64pp. Woods Hole. Massachusetts.
- Uppala, S.M., and Co-authors, 2005: The ERA-40 re-analysis. *Quart. J. R. Meteorol. Soc.*, **131**, 2961-3012.
- Zhang, G. J., and McFarlane, N. A. 1995: Sensitivity of climate simulations to the parameterization of cumulus convection in the Canadian Climate Centre Circulation Model. *J. Atmos. Sci.* **33**, 407-446.
- Zhang, G, and Mu, M. 2005: Simulation of the Madden-Julian Oscillation in the NCAR CCM3 using a revised Zhang-McFarlane convection parameterization scheme. *J. Climate*, **18**, 4046-4064.
- Zhu, H., Hendon, H. and Jacob, C. 2009: Convection in a parameterized and super-parameterized model and its role in the representation of the MJO. *J. Atmos. Sci.*, **66**, 2796-2811.



The Centre for Australian Weather and Climate Research is a partnership between CSIRO and the Bureau of Meteorology.